Draft version February 18, 2025
Typeset using LaTeX default style in AASTeX631

Observation-Based Iterative Map for Solar Cycles. I. Nature of Solar Cycle Variability

Zi-Fan Wang,[1] Jie Jiang,[2,3] and Jing-Xiu Wang[4,1]

[1] *Key Laboratory of Solar Activity, National Astronomical Observatories, Chinese Academy of Sciences, Beijing 100101, China*
[2] *School of Space and Environment, Beihang University, Beijing, China*
[3] *Key Laboratory of Space Environment Monitoring and Information Processing of MIIT, Beijing, China*
[4] *School of Astronomy and Space Science, University of Chinese Academy of Sciences, Beijing, China*

ABSTRACT

Inter-cycle variations in the series of 11-year solar activity cycles have a significant impact on both the space environment and climate. Whether solar cycle variability is dominated by deterministic chaos or stochastic perturbations remains an open question. Distinguishing between the two mechanisms is crucial for predicting solar cycles. Here we reduce the solar dynamo process responsible for the solar cycle to a one-dimensional iterative map, incorporating recent advance in the observed nonlinearity and stochasticity of the cycle. We demonstrate that deterministic chaos is absent in the nonlinear system, regardless of model parameters, if the generation of the poloidal field follows an increase-then-saturate pattern as the cycle strength increases. The synthesized solar cycles generated by the iterative map exhibit a probability density function (PDF) similar to that of observed normal cycles, supporting the dominant role of stochasticity in solar cycle variability. The parameters governing nonlinearity and stochasticity profoundly influence the PDF. The iterative map provides a quick and effective tool for predicting the range, including uncertainty of the subsequent cycle strength when an ongoing cycle amplitude is known. Due to stochasticity, a solar cycle loses almost all its original information within 1 or 2 cycles. Although the simplicity of the iterative map, the behaviors it exhibits are generic for the nonlinear system. Our results provide guidelines for analyzing solar dynamo models in terms of chaos and stochasticity, highlight the limitation in predicting solar cycle, and motivate further refinement of observational constraints on nonlinear and stochastic processes.

1. INTRODUCTION

The 11-year solar activity cycle is the most prominent feature of the solar magnetic field (Hathaway 2015). Usually indicated by the peak sunspot number during one cycle, the cycle amplitudes vary within a vast range, including periods of very low activity such as the Maunder Minimum (Eddy 1976), and periods of high activity such as the Modern Maximum (Lean et al. 1995). Moreover, the normal cycles exhibit a weak-strong alternating tendency, known as the Gnevyshev-Ohl rule (G-O rule, Even-Odd effect) (Gnevyshev & Ohl 1948). These variations shape the observed solar cycle, which may seem random but reveals key semi-regular patterns. These patterns offer valuable insights into cycle prediction and space climate research.

It is widely accepted that a solar dynamo process is responsible for the origin and evolution of solar cycles (Charbonneau 2020). The nonlinearity and stochasticity of the solar dynamo are key to explaining cycle variability, including the range of cycle amplitudes and semi-regular patterns like the G-O rule. Solar dynamo explains the solar cycle as the mutual generation of toroidal magnetic field and poloidal field (Parker 1955; Steenbeck et al. 1966; Parker 1979). The solar dynamo is evident to be of Babcock-Leighton (B-L) type (Cameron & Schüssler 2015), in which the generation of toroidal field from poloidal field is generally linear. The linear relationship is supported by the polar field precursor for cycle prediction as the polar field at cycle minimum is taken as the representative of the poloidal field (Ohl & Ohl 1979; Svalgaard et al. 2005; Schatten 2005). Besides the linear part, solar dynamo also contains nonlinear mechanisms to confine the amplitude range (Yoshimura 1978a), making the next cycle weaker for strong cycles, similar to the G-O

Corresponding author: Jie Jiang
jiejiang@buaa.edu.cn

rule. Earlier studies suggested that certain nonlinear feedback mechanisms can cause dynamo models to undergo a clear transition to chaos, marked by a sequence of period-doubling bifurcations (Yoshimura 1978b; Schmalz & Stix 1991; Charbonneau et al. 2005). Such deterministic chaos may explain the irregularities of solar cycle variations. Meanwhile, as the generation of poloidal field from toroidal field happens in the convection zone (Parker 1955), the stochasticity arising from turbulent convection also influences the solar cycle evolution, probably generating irregular cycle amplitude variations.

Whether deterministic chaos or stochasticity causes the solar cycle variability is yet to be answered. Some attempts on analysis of time series of solar activity proxies (Mundt et al. 1991; Rozelot 1995; Hanslmeier & Brajša 2010; Deng et al. 2016) or investigations based on dynamic equations (Tobias et al. 1995; Knobloch et al. 1998; Charbonneau 2001; Wilmot-Smith et al. 2005) suggest that solar cycle variability is due to deterministic chaos subject to weak stochastic perturbations. In contrast, with similar methods, some studies (Price et al. 1992; Carbonell et al. 1994; Mininni et al. 2000; Kitchatinov & Olemskoy 2016; Cameron & Schüssler 2017) demonstrated that solar cycle variability results from weakly nonlinear limit cycle affected by stochastic perturbations. Understanding the nature of solar cycle variability is a prerequisite for reasonably predicting future solar cycles (Petrovay 2020), and is also the prototype for understanding stellar variability.

While certain properties of solar dynamo and the nature of cycle variability can be evaluated by kinematic or even fully magnetohydrodynamic simulations (Charbonneau 2020; Karak 2023), simplifying the dynamo into an iterative map of cycle amplitudes provides an effective and convenient method for evaluating their properties in the presence of dominant chaos or stochasticity, as long as the nonlinearity and stochasticity are realistically quantified (May 1976; Charbonneau et al. 2005). Pioneered by Durney (2000) and Charbonneau (2001), iterative maps of solar cycles are not as developed as other methods, but more recent progress on solar dynamo can revive such iteration map studies.

Within the B-L type dynamo, the generation of poloidal field from toroidal field results from the emergence of tilted active regions and their subsequent surface flux transport evolutions (Wang & Sheeley 1991; Jiang et al. 2013; Petrovay et al. 2020; Yeates et al. 2023). Such surface evolution process can be observationally confined. Studies on historical datasets indicate that with increasing cycle strength, the average tilt angle decreases (Dasi-Espuig et al. 2010; Jiao et al. 2021) and the average latitude increases (Li et al. 2003; Solanki et al. 2008), which consequently limits the generation of poloidal field. This B-L type nonlinearity can effectively modulate the polar field generation (Jiang 2020; Karak 2020; Talafha et al. 2022; Yeates et al. 2024). Meanwhile, as the rise of toroidal flux through the convection zone to form active regions is buffeted by the turbulent convection (Weber et al. 2013), the latitude and tilt are always of large scatter (Jiang et al. 2011a, 2014a). This observation-based B-L stochasticity can modulate solar cycles, the relative importance of which has been evaluated recently (Jiang 2020; Talafha et al. 2022; Kumar et al. 2024).

The observations and theoretical studies of B-L dynamo make it possible to create a realistic recursion relation between the amplitude of adjacent cycles. Following the quantification of B-L type nonlinearity and stochasticity by Jiang (2020) (hereafter J20), we create an iterative map of solar cycle amplitudes. In this paper, as the first of the iterative map series, we perform an analysis of the origin of solar cycle variability, answer whether deterministic chaos or stochasticity dominates the variability, and investigate how nonlinearity and stochasticity of different strength affect the variability, by evaluating the properties of the solar cycle iterative map. We will continue evaluating the Gnevyshev-Ohl rule using the iterative map in a subsequent paper. In the third paper, we will first validate the iterative map for solar cycle prediction and then apply it to predict the range of solar cycle 26, based on the amplitude of cycle 25.

The paper is organized as follows. In Section 2 we construct the iterative map and describe its parameters. In Section 3 we analyze the origin of cycle variability and the distribution of cycle amplitudes from series of cycle amplitudes synthesised from the iterative map. We discuss the implication for cycle prediction of our results in Section 4. We conclude our paper in Section 6.

2. ITERATIVE MAP OF SOLAR CYCLE AMPLITUDES

The B-L type dynamo offers a framework for establishing a relationship between successive solar cycles, in which the generation of the poloidal field from toroidal field can be constrained by observations. Durney (2000) and Charbonneau (2001) first constructed a nonlinear recursion function of solar cycle amplitude based on the B-L type dynamo. We adopt this methodology, incorporating recent understandings of the B-L mechanism, particularly those presented by J20, to create the 1D iterative map for cycle-to-cycle amplitude variations. The map enables us to explore the nature

the solar cycle variability using established tools from nonlinear dynamics, such as fix-point stability and cobweb diagrams.

The solar dynamo process is composed of the mutual generation of poloidal and toroidal field. The poloidal field at cycle minimum is crucial in B-L dynamo for being the seed of the following cycle. We use its analog, the axial dipole moment of surface field at cycle minimum, which is denoted as $DM\,(n)$ for the dipole moment at the end of n-th cycle. As for the toroidal field during the solar cycle, it can be represented as the cycle amplitude which describes the active region emergence during the cycle, denoted as $SN\,(n)$ for the n-th cycle.

We begin with the first assumption that the generation of toroidal field, i.e. the Ω-effect, is mostly linear and less noisy compared to other processes. This corresponds to the polar field precursor mentioned in Section 1. This is written as follows,

$$SN\,(n) = k_0 DM\,(n-1)\,, \tag{1}$$

in which k_0 is the linear coefficient that describes the strength of the Ω-effect and can be derived from the observed solar cycle amplitude and the surface magnetic field at cycle minima.

We then consider how the poloidal field is in turn generated from the toroidal field. Originally, Durney (2000) suggested that the newly generated poloidal field, or $DM\,(n)$ in our notation, is a certain function of the toroidal field, or $SN\,(n)$ in our notation. However, as the B-L mechanism suggests, during the solar cycle n, originating from active regions, the surplus flux of opposite sign to the polar field migrates poleward, causes polar field reversal before building up the polar field at the next cycle minimum. This imply that, instead of directly generating $DM\,(n)$, the total toroidal field during cycle n, represented by $SN\,(n)$, is actually generating the difference between adjacent DMs, as shown by the following,

$$\Delta DM(n) = DM\,(n) + DM\,(n-1)\,, \tag{2}$$

where $\Delta DM(n)$ is a function of $SN\,(n)$, representing the total amount of dipole moment at cycle minimum contributed by all the active regions during cycle n. The values of DM and SN we use in this article are all positive, and thus it is the positive sign in the equation. Here we include the second assumption that Hale's polarity law is always kept, so that the new dipole moment always cancels out with the old.

Combining Equations (1) and (2), a complete recursion relation between adjacent cycles can be obtained if a certain form of ΔDM is given. Unlike Durney (2000) and Charbonneau (2001), who introduced a parameter to represent the strength of the nonlinearity without specifying its physical origin, we base our approach on the results of J20, which offer a clear interpretation and quantification of the nonlinearity in the B-L dynamo. Using empirical rules of AR emergence, and surface flux transport simulations, J20 shows that ΔDM follows a nonlinear function of $SN\,(n)$. J20 includes tilt quenching and latitude quenching as B-L nonlinearity, and the scatter of active region properties as B-L stochasticity. ΔDM follows a increase-then-saturate pattern as the increase of cycle amplitude, which means that the generation of poloidal field increases when cycle amplitude increases from weak to strong, but does not increase or decrease when the cycle becomes even stronger. This is different from increase-then-decrease pattern, such as the results of Charbonneau (2001) where there is a decreasing part after the cycle becomes too strong. The saturated pattern of J20 primarily arises from the similar decay properties of solar cycles in sunspot numbers (Cameron & Schüssler 2016; Jiang et al. 2018; Biswas et al. 2022).

The J20 form of ΔDM is written below, with a deterministic case including only nonlinearity and a stochastic case including both nonlinearity and stochasticity.

$$\Delta DM = \begin{cases} k_1 \mathbf{erf}\left(\frac{SN(n)}{quench}\right) & \text{deterministic case;} \\ k_1 \mathbf{erf}\left(\frac{SN(n)}{quench}\right)(1 + stoch \times X) & \text{stochastic case,} \end{cases} \tag{3}$$

where **erf** is the error function. The parameter k_1 represents the saturated value of the total dipole moment ΔDM contributed by all ARs during a strong solar cycle. The parameter *quench* determines the rate at which ΔDM saturates as a function of sunspot number $SN\,(n)$ of cycle n. Finally, the parameter X is a normally distributed random variable with a standard deviation given by *stoch*. Figure 4 of J20 illustrates the dependence of ΔDM on $SN\,(n)$.

With the realistic ΔDM, the recursion function of cycle amplitudes can be finalized. The deterministic case is as follows,

$$SN\,(n+1) = k_0 k_1 \mathbf{erf}\left(\frac{SN\,(n)}{quench}\right) - SN\,(n)\,, \tag{4}$$

while the stochastic case is

$$SN\,(n+1) = k_0 k_1 \mathbf{erf}\left(\frac{SN\,(n)}{quench}\right)(1 + stoch \times X) - SN\,(n)\,. \tag{5}$$

These two cases can be used to generate series of solar cycle amplitudes for analysis efficiently when an initial condition is given. Meanwhile, they can also be used to predict solar cycles with a given $SN\,(n)$, including uncertainties of prediction.

The parameters in Equation (5) are obtained from observations and surface flux transport simulations. The parameter $k_0 = 58.7$ (Jiang et al. 2018) for the linear Ω-effect is derived from the linear relationship between the axial dipole moment (based on WSO, MWO, MDI/SOHO, and HMI/SDO synoptic magnetograms at the cycle $n-1/n$ minimum) and the maximum value of the 13-month smoothed monthly sunspot number over cycle n in Sunspot Number Version 2. For the nonlinear and stochastic B-L mechanism, the parameters need to be obtained by simulating the surface flux transport of ARs following observational properties, like J20 did. We adopt the parameters of J20, with maximum dipole moment k_1 being 6.94, *quench* being 75.85, and *stoch* being 0.17, in order to analyze the nature of cycle variability. This parameter set is referred to as the standard set.

We note that the cycle amplitude $SN(n)$ used in this paper is the widely adopted maximum value of the 13-month smoothed monthly sunspot number for cycle n (Hathaway 2015), rather than an integrated value. The maximum value of sunspot number is approximately proportional to the total sunspot area (Balmaceda et al. 2009) and total magnetic flux (Jiang et al. 2011b), which are directly related to the toroidal field during a solar cycle. While the detailed evolution of the cycle may slightly influence the total toroidal field, we do not account for these variations in our current approximation.

The parameters have uncertainty because of the limitations of observational and statistical study of ARs and surface flows. The uncertainty of ARs and flows then affect the production of ΔDM by surface flux transport processes (Jiang et al. 2014b; Yeates et al. 2023), and should be examined with numerical simulations. In this paper, we do not examine the quantity of model parameter uncertainty caused by uncertainty of ARs and flows. Instead, we introduce a considerable range of parameters and study their influence on the solar cycle variability.

3. NATURE OF SOLAR CYCLE VARIABILITY

3.1. *No deterministic chaos in cycle variability*

With the recursion relation of $SN\,(n)$ originated from B-L dynamo, the role of nonlinearity and stochasticity in the solar cycle evolution and whether chaos is present can be evaluated by analyzing the recursion function and the synthesised solar cycle amplitude series.

To determine whether determinisitic chaos is present, we first analyze the determinisic case without stochasticity. The characteristics of the fixed point of the recursion function is critical to chaos. We begin with analyzing the recursion function with the standard parameters, shown by the black curves in Figure 1 a. As the panels show, the recursion function has 1 fixed points except the origin. It is commonly known that the stability of a fixed point is determined by the derivative. That is, let $f\,(x)$ be the recursion function of $\{x_n\}$, then a fixed point x^* is stable if $\left|f^{'}\,(x^*)\right| < 1$. From Figure 1 a, the fixed point is on the decreasing part of the recursion function, so the derivative is obviously smaller than 1. Meanwhile, since the derivative of the deterministic case can be written as,

$$\frac{dSN\,(n+1)}{dSN\,(n)} = \frac{2k_0k_1}{\sqrt{\pi}quench}\exp\left(-\left(\frac{SN\,(n)}{quench}\right)^2\right) - 1, \tag{6}$$

it can be clearly seen that it is always larger than -1. Then we know that the fixed point has the absolute value of derivative smaller than 1, indicating that it is stable. A stable fixed point results in converging into the fixed point instead of chaos for the deterministic case. More generally, Equation (6) follows,

$$\left|\frac{dSN\,(n+1)}{dSN\,(n)}\right|_{SN(n)=x^*} < 1, \quad \forall\ k_0, k_1, quench, \tag{7}$$

which implies that the nonzero fixed point is stable regardless of parameters. Again, it is easy to know from Equation (6) that $\frac{dSN(n+1)}{dSN(n)} > -1$. Meanwhile, in order to have 1 nonzero fixed point, $\frac{dSN(n+1)}{dSN(n)} > 1$ should hold at the origin. Then, it can be easily know that $\frac{dSN(n+1)}{dSN(n)} < 1$ at the nonzero fixed point, thus confirming Equation (7).

From a larger perspective, this result is not only limited to ΔDM following Equation (3). If ΔDM follows a increase-then-saturate form, which means that its derivative is large at the start, and gradually decreases, finally approaching the limit 0. That is, $\frac{d\Delta DM}{dSN} > 0$ while $\frac{d^2\Delta DM}{dSN^2} < 0$ if these derivatives exist. For such kind of ΔDM with gradually decreasing derivative, the recursion function of cycles is concave and is easy to know that the nonzero fixed point has derivative smaller than 1 if the origin has derivative larger than 1 (we can assume that the derivative at the origin should be larger than 1 so that weak solar cycles would not converge to 0). Meanwhile, the derivative of recursion function becomes closer to but always larger than -1 as the cycle amplitude increases. Therefore, such a general kind of poloidal field generation mechanism has stable fixed point, which imply that they do not have chaos.

The absence of chaos implies that the initial uncertainty will not be enlarged exponentially. This is characterized by the Lyapunov exponent, so we calculate the Lyapunov exponent of different k_1 and *quench* for the iterative map following Equation (4). The exponent is obtained from a series of 5000 cycles for each parameter set, with the initial cycle amplitude being 150. The result is displayed by Figure 2, which clearly presents 2 strips of negative values. For larger k_1 and smaller *quench* values, the exponent falls to almost 0, indicating extremely slow convergence to the fixed point. Positive values are not observed in the figure, hence no chaos is present in the model for the parameter range we concern, that is, tiny difference between initial conditions will not grow unbounded.

To show the absence of chaos more clearly and intuitively, we generate series of cycle amplitudes and plot cobweb diagrams to show their iterations. We generate series of the deterministic case as expressed by Equation (4). The standard parameter set is used. We consider 3 initial cycle amplitudes $SN\,(0) = 50$, 150, and 250, covering both below and above the fixed point where $SN\,(n+1) = SN\,(n)$ shown in Figure 1a. Then, the iterations starting from 3 initial conditions are shown with folding lines in cobweb diagrams along with the recursion functions and diagonal lines, as shown in Figures 1a, respectively.

The 3 series of cycle amplitudes of the deterministic case are not chaotic. The corresponding cycle amplitude evolutions for the first 50 cycles are plotted in Figures 1a, c. All show regular alternating strong and weak patterns with amplitude slowly converging to the fixed point. As shown in Figure 1c, the convergence is slower for points closer to the fixed point. The slow convergence results from Equation (6) being only slightly larger than -1 near the fixed point, and also corresponds to the near 0 value of Lyanpuov exponent shown in Figure 2. The diagrams clearly illustrate that the deterministic case does not possess chaos.

Since chaos is not present in the model, stochasticity should be the primary source of cycle variability, To show this, we generate a series of cycles and corresponding cobweb diagrams for the stochastic case. We use recursion function Equation (5) and initial amplitude 150, generate a series of cycle amplitudes, and plot the cycle evolution in Figures 1b and 1d. The recursion function now exhibits a large scatter range compared to the deterministic case, and the iterations of the Cobweb diagram expanse across the displayed range. The irregularities of cycle evolution are clear for the stochastic case, while converging behavior is not observed, different from the deterministic case. The varying solar cycle amplitudes look similar to observations, suggesting that stochastic processes could be the main cause of solar cycle variability.

For the stochastic case, the predictability of the cycle amplitude is strongly limited by $k_1 stoch$. From Equation (3), the scatter of the next cycle for cycle n is $k_0 k_1 stoch\mathbf{erf}\left(\frac{SN(n)}{quench}\right)$, which is already notably diverging for the same $SN\,(n)$ as shown by the gray scale shade in Figure 1 (b). Therefore, the predictability is always limited, and Lyapunov exponent is not needed for this case. We will further discuss the predictability of solar cycles when stochasitcity is considered in Section 4.

3.2. *The probability density distribution of cycle amplitudes*

It is important to examine whether the varying cycle amplitudes generated by the stochastic case follow realistic statistical properties. We analyze the probability density distribution of the solar cycle amplitude produced by the stochastic case. Using the standard parameter set, we generate 1,000,000 cycle amplitudes, and obtain their probability density function (PDF). We then compare the results with the PDF of the long-term solar activity reconstructed from radioisotopes by Usoskin et al. (2014). However, before comparison, we need to convert Usoskin et al. (2014)'s results to match our convention.

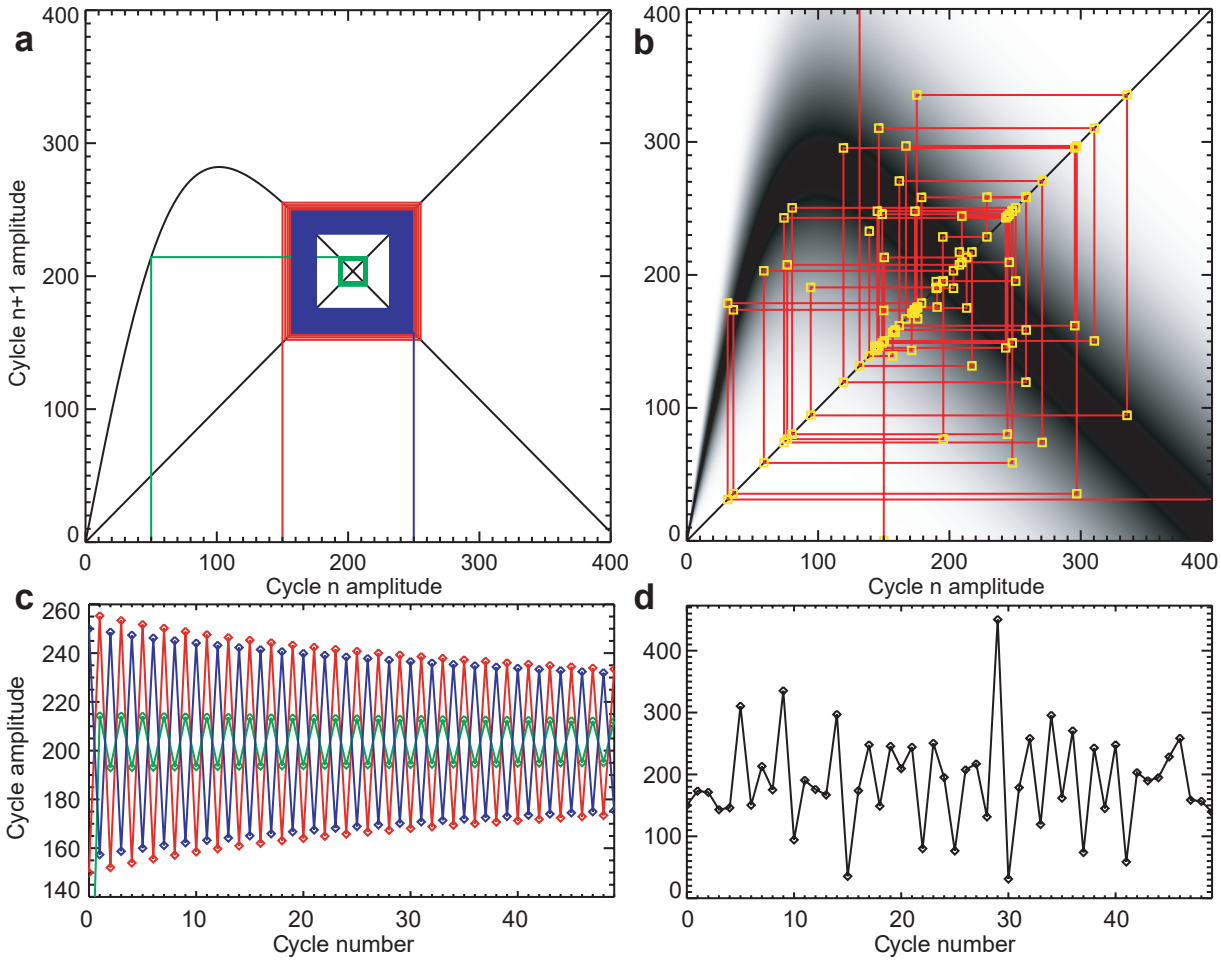

Figure 1. Generation of solar cycle amplitudes with Cobweb diagrams. **a,** The Cobweb diagram for the deterministic case, with the black curve representing the recursion function Equation (4). The green, red, and blue curves represent the evolution of cycle amplitude with initial amplitudes of 50, 150, and 250, respectively. The corresponding cycle series is presented in Panel c. The diagonal black line represents $SN\,(n) = SN\,(n+1)$. **b,** The Cobweb diagram for the stochastic case. The gray-scale shade represents the probability distribution of the iterative map, with deeper being more likely. Yellow squares indicate possible amplitudes of the cycle series, which are presented in Panel d. **c,** Cycle amplitude evolution for the deterministic case. The green, red, and blue curves are the evolution of cycle amplitude from Panel a. **d,** Cycle amplitude evolution for the stochastic case in Panel b.

Usoskin et al. (2014) express the long-term solar activity variations as 10-year average of sunspot numbers, instead of the maximum sunspot number during a cycle. Moreover, Usoskin et al. (2014) use a sunspot number series different from J20 which we mainly adopt. To compensate these, we first need to find the relationship between cycle amplitude defined by the maximum sunspot number during a cycle and the 10-year average sunspot number. To simplify the method, we assume that the 10-year average is analogous to solar cycle average. Usoskin et al. (2021) contains resolved solar cycles in the recent millennium. We find the cycle maximum sunspot number (the cycle amplitude we use) and the cycle average sunspot number from their results, as well as the corresponding measure errors. There are 85 cycles in total, shown in Figure 3. The two sunspot number series follow a linear relationship, so we perform a linear fit (Markwardt 2009). The relationship between average sunspot number SN_{ave} and maximum sunspot number SN_{max} is then $SN_{max} = (1.95 \pm 0.08)\,SN_{ave} + (24 \pm 2)$. The χ^2 of the fit is 94.

The cycle amplitudes of Usoskin et al. (2014) is compared to the Group Sunspot Number series (Hoyt & Schatten 1998), which is scaled to the Wolf Sunspot Number since 1874. The version 2.0 of the International Sunspot Number can be regarded as the Wolf Sunspot Number divided by 0.6 (Clette et al. 2014). Hence, we also use a factor of 1/0.6

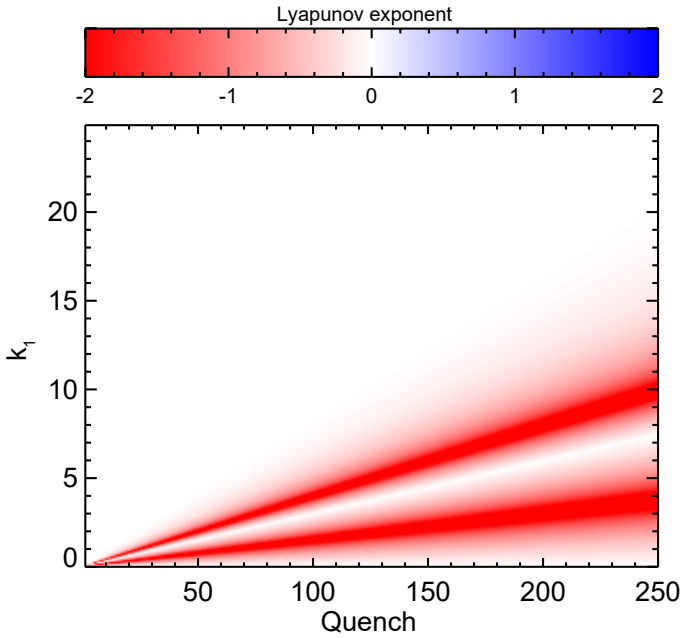

Figure 2. Lyapunov exponents for various ranges of the parameters *quench* and k_1.

when we compare our results with the results of Usoskin et al. (2014). The relationship is as follows,

$$SN = \left[(1.95 \pm 0.08)\, SN_{Usoskin} + (24 \pm 2)\right] / 0.6, \tag{8}$$

and we use this to convert the data when we compare the PDF of the model with observations.

Using the stochastic case of recursion function, we generate 1,000,000 solar cycle amplitudes and obtain the corresponding PDF, shown by the red curve in Figures 4 a-c. Since our method is based on the empirical properties of the ARs used in J20, only the amplitudes larger than the weakest observed cycle used in J20 (cycle 14 with amplitude 107.1) are constrained by observations, marked by the part to the right of the dashed line. Qualitatively, the PDF curves consist of a single peak similar to the normal cycle component in the PDF of Usoskin et al. (2014) shown in black. However, at low cycle amplitudes to the left of the dashed line, i.e., grand minima, the curves differ from Usoskin et al. (2014) because they do not have the grand minima component. Quantitatively, the peak amplitude is approximately 200, which is within 11% of the reconstructed normal cycle component in the PDF of Usoskin et al. (2014). The peak probability density and distribution width are less consistent with the reconstructed results, though. The quantitative difference to observations is likely due to the uncertainty of nonlinearity and stochasticity parameters.

The PDF of synthetic cycle amplitude varies with nonlinearity and stochasticity parameters. We consider a ±25% variation of each parameter, changing one parameter at a time while keeping others unchanged. Thus 6 cases are considered: $0.75 \times k_1$, $1.25 \times k_1$, $0.75 \times$ *quench*, $1.25 \times$ *quench*, $0.75 \times$ *stoch*, and $1.25 \times$ *stoch*. The influence of parameter difference can then be obtained by comparisons of different series generated from the 6 parameter sets.

The PDFs of the 6 parameter sets are shown in different colors in Figures 4a-c. Among the 3 parameters, the maximum dipole moment k_1 has the greatest influence on the PDF. It significantly impacts both the peak cycle amplitude and the width of the distribution, making it the most critical factor in determining the overall behavior. The result of $0.75 \times k_1$ is more consistent with the reconstructed PDF of Usoskin et al. (2014) in terms of both peak amplitude and peak probability density. The other parameters primarily affect the width, and have less influence on the peak amplitude. A smaller *quench* or larger *stoch* results in a wider peak, while having a minor effect on the peak cycle amplitude. We note that, since the stochastic component is multiplicative to ΔDM, the actual scattering range is generally larger for larger k_1 value, and hence a wider PDF curve.

Knowing how the PDF is affected by the parameters, we can then show how the nonlinearity and stochasticity in reality may be different from that of J20. We modify the parameters and look for a closer match to Usoskin et al. (2014). The close match shown by the orange curve in Figure 4d is obtained by modifying the parameters together.

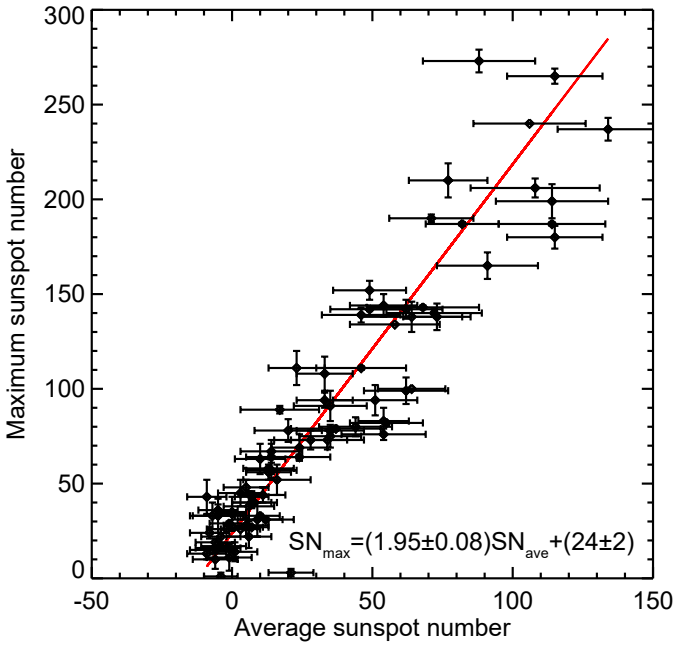

Figure 3. Relationship between cycle average sunspot numbers and cycle maximum sunspot numbers. Each diamond represents a solar cycle, the error bars represent standard error, and the line represents linear fit. In total, 85 cycles occurred between the years 791 and 1900.

This indicates that compared to results of J20, the B-L type dynamo may saturate at higher cycle amplitudes, but the saturated dipole moment should be smaller. Meanwhile the stochasticity might be a little less. For simplicity, this parameter set is made by some trials instead of parameter optimization, so it may not be the best fit, or the most realistic fit. Still, it should be warned that the reconstructed sunspot numbers by Usoskin et al. (2014) has uncertainty as well, which may affect the evaluation of our results.

4. IMPLICATIONS FOR SOLAR CYCLE PREDICTION

The iterative map of cycle amplitudes generates the amplitude of the next cycle along with its uncertainty when the current cycle amplitude is given. This can be regarded as cycle prediction of the next cycle. The cycle amplitude can be obtained when the cycle has reached its maximum. If we use the maximum International Sunspot Number 2.0, and suppose that cycle 25 is already close to maximum, which is approximately 140, we can then produce a prediction of cycle 26. Using Equation (5) and the standard set of parameters, we get that the amplitude of cycle 26 will be 264 with 1σ uncertainty being 45. If we use the parameter set in Figure 4d, which is more close to the observational PDF, the amplitude of cycle 26 will be 197 with 1σ uncertainty being 25. This implies that iterative map can provide a efficient and simplified means for cycle prediction, only if the properties of the dynamo can be realistically quantified.

Our results show that the stochasticity is the primary source of cycle variability, and a realistic quantity of stochasticity is needed to form a PDF of cycle amplitudes similar to observations. While the stochasticity may be weaker than the standard parameters we use, the difference should not be of several magnitudes. Although the observational studies of the active region emergence is possibly still yet to be refined, it is certain that the stochasticity shall play an important role in cycle prediction.

Since stochasticity itself is intrinsically not predictable, it naturally limits the effective range of solar cycle prediction. While predicting the next cycle at exactly the cycle minimum can be correct, prediction before the cycle minimum always has a uncertainty range which increases as we make prediction at earlier stage of cycle evolution, as shown by Jiang et al. (2018), because stochasticiy is involved.

For prediction beyond 1 cycle, the effect of stochasticity is even stronger, and long-term prediction is not valid from this perspective. The recursion function itself already has a large uncertainty, and this inherent uncertainty affects cycle predictions at each iteration. To give an example, we start at SN(0) = 140, which approximates the

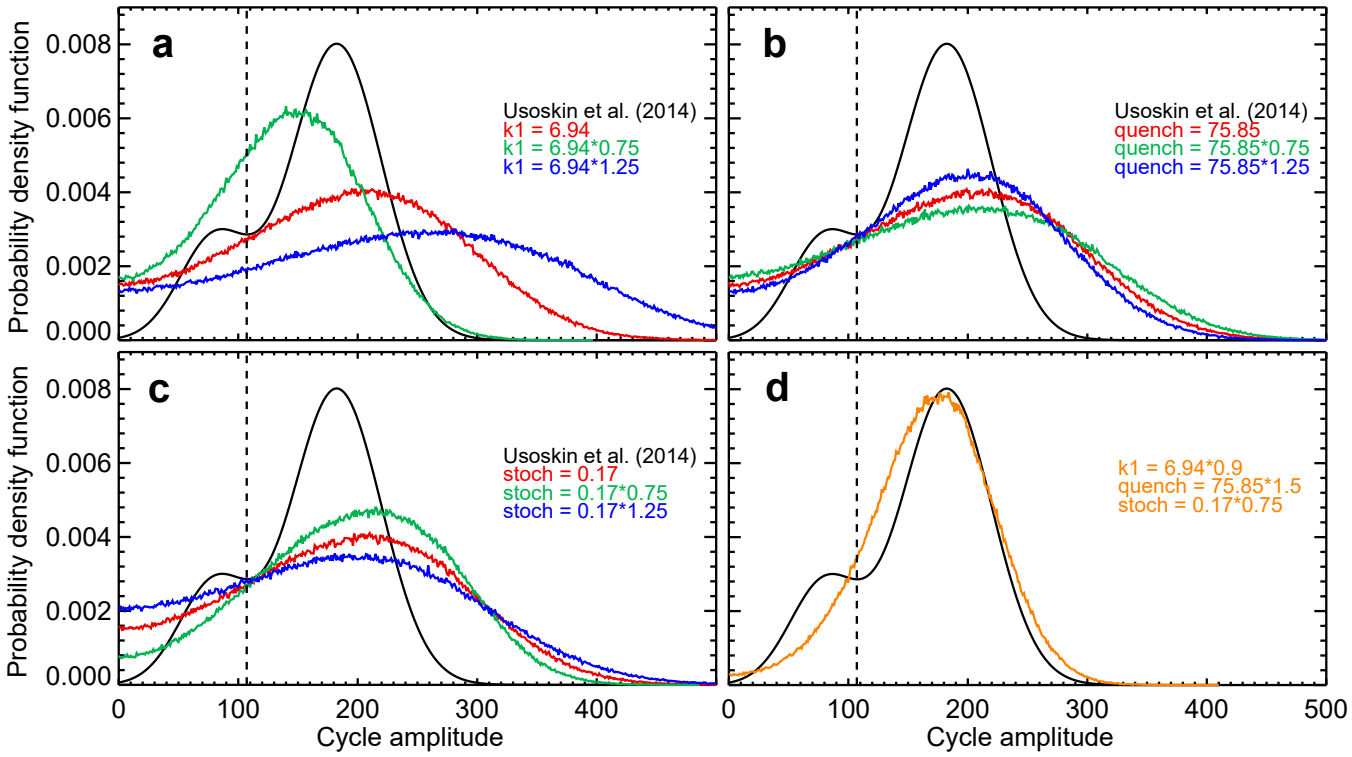

Figure 4. PDFs of cycle amplitude, under different parameter sets. **a-c,** Modified k_1, *quench*, and *stoch* respectively, with different colors displaying different parameters as stated in the panels. **d,** A case that modifies both k_1 and *quench*, displayed in orange. The black curves are from Usoskin et al. (2014). The black dashed vertical line marks the weakest cycle amplitude 107.1 to deduce the empirical rules of ARs in J20.

the amplitude of cycle 25, produce several sets of cycle amplitude series using the standard set of parameters, and calculate the standard deviations of SN(n), which corresponds to the uncertainty of cycle prediction ahead of n cycles. As shown in Figure 5, the standard deviation of SN(n) increases rapidly, and soon saturates after 3 or 4 cycles, where the standard deviation agrees with the cycle amplitude variations illustrated by the PDF in Figure 4. This indicates that in our model, the uncertainty of long-term cycle prediction is too large for it to be meaningful. A solar cycle quickly loses all of its original information after a few iterations and becomes completely indistinguishable from any solar cycle among the entire PDF of cycles. This loss of distinction is a direct consequence of stochastic processes.

5. DISCUSSIONS

The iterative map is a well-established tool in the field of nonlinear dynamics. It facilitates the analysis of solar cycle variability and helps us explore the nature of the dynamic system governing solar dynamo processes. Despite its simplicity, the nonlinear behaviors it reveals are generic (May 1976). Using the BL-type dynamo, Charbonneau et al. (2005) confirmed that low-order dynamical systems can capture essential features of the full problem. The key challenge lies in realistically constructing the nonlinearity and stochasticity that characterize the solar cycle system.

Durney (2000); Charbonneau (2001) once presented iteration maps of solar cycle amplitudes. They demonstrated that, for certain parameter ranges, the solar dynamo could enter a chaotic regime, which contrasts with our findings. The discrepancy stems from the different forms of nonlinearity used. In the earlier studies, functions with free parameters were introduced to represent nonlinearity, without clearly specifying their physical origin. In contrast, we adopt forms of nonlinearity and stochasticity with well-defined interpretations and quantifications, based on the work of J20. This approach marks a clear advancement over previous studies. Other reason for the discrepancy lies in how the poloidal field, generated by the toroidal field of cycle n (denoted as ΔDM), is treated. In the earlier studies, ΔDM was mistakenly assumed to be equivalent to the dipole moment strength at the end of cycle n, i.e.,

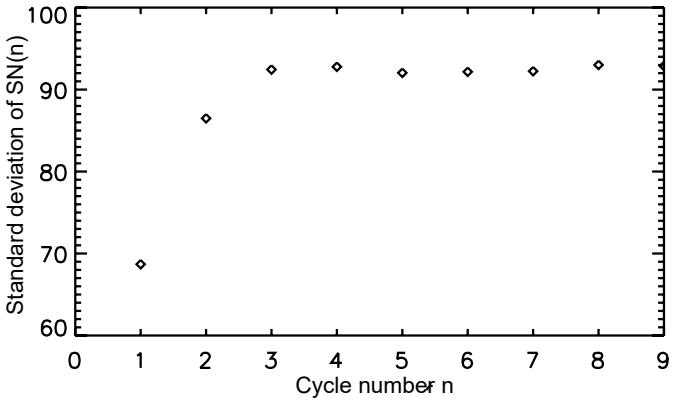

Figure 5. The standard deviation of SN(n) when SN(0) is 140. Each standard deviation is calculated from 10,000 SN(n) values.

$\Delta DM = DM\,(n)$. In reality, ΔDM must first cancel out the residual poloidal field from the previous cycle, meaning it should be expressed as $\Delta DM = DM\,(n) + DM\,(n-1)$. The two major differences lead to fundamentally distinct interpretations of solar cycle variability when analyzed through iterative maps.

Our findings, which indicate the absence of chaos and the stochastic origin of solar cycle variability, agree with Cameron & Schüssler (2017), who attribute solar cycle variability to a weakly nonlinear limit cycle affected by random noise. Comparing to the model of Cameron & Schüssler (2017) considering a B-L dynamo in general, we introduce the nonlinearity and stochasticity based on observational latitude and tilt quenching of active regions analyzed in J20. Such observation based nonlinearity cannot produce chaos regardless of parameters. Generally, any α-effect following an increase-then-saturate form cannot produce chaos. It is the similar decay properties of solar cycles in sunspot numbers that mainly leads to the saturate form of the α-effect (Cameron & Schüssler 2016; Jiang et al. 2018; Biswas et al. 2022). While it has been shown that stochastic dynamo models can produce certain properties of cycle variability in previous works (e.g., Charbonneau & Dikpati 2000; Passos et al. 2014), we clearly show that why nonlinearity should not be the origin of cycle variability in a generic method.

In our model, there is no modulation beyond 1 cycle, and it does not present long-term memory. Successful cycle predictions for the weak cycle 24 using precursor methods (Svalgaard et al. 2005; Schatten 2005) and solar dynamo models (Choudhuri et al. 2007; Jiang et al. 2007) have suggested that the memory of solar dynamo model is limited to within 1 cycle. The predictions of a stronger cycle 25 compared to cycle 24, made by surface flux transport based models (e.g., Cameron et al. 2016; Jiang et al. 2018; Jiang & Cao 2018) and dynamo based models (e.g., Bhowmik & Nandy 2018; Guo et al. 2021) also provide supporting evidence. Meanwhile, power spectra derived from the 1,000,000 solar cycle series generated based on the iterative map show no significant peaks around 8 cycles, which corresponds to the Gleissberg period (Gleissberg 1939). This aligns with the finding of Cameron & Schüssler (2019), who have also shown that long-term modulation is not needed to explain the solar cycle variability when stochastic forcing is present. Based on this, we argue that the iterative map, which lacks long-term memory, is a reasonable representation of solar cycle amplitude evolution, and longer-than-1-cycle modulations are not a primary concern as we evaluate the effects of nonlinearity and stochasticity. As for the G-O rule, our model possesses G-O rule behavior when the cycle series are paired up. More pairs tend to be constructed by a weaker cycle followed by a stronger cycle instead of the opposite. This phenomenon is a result of the PDF that the cycles follow as shown in Figure 4, and the recursion function Equation (5). We will focus on the G-O rule and provide a more detailed examination and clearer definitions of it in the subsequent paper in this series.

Nonlinearity and stochasticity are key factors controlling the probability density distribution of cycle amplitudes. The mode of the distribution is primarily determined by the maximum dipole moment generated by active regions, while the width of the distribution is influenced by both nonlinearity and stochasticity. Uncertainties in the parameters of nonlinearity and stochasticity arise from the limitations of observational constraints on the B-L type dynamo, posing challenges when comparing with observations. As summarized by Jiao et al. (2021), previous studies on tilt quenching have shown inconsistencies due to difference in datasets and methods. Recently, Qin et al. (2024) decrease

measurement errors in tilt angles through mutual validation of datasets, enabling a more accurate analysis of their intrinsic properties. Although dynamo quenching due to AR properties is becoming clearer, further investigation is still needed. Meanwhile, Petrovay et al. (2020); Wang et al. (2021) suggest that near-equator meridional flows and surface turbulent diffusion also influence the contribution of ARs to solar cycle evolution. Variations in AR and flow properties will yield different parameters in our model, affecting the distribution of cycle amplitudes. In addition to uncertainties in the observed nonlinearity and stochasticity of B-L type dynamo, uncertainties in reconstructed sunspot numbers also limit the statistical conclusions.

While the recursion function for normal cycles is subject to parameter uncertainty, it is completely unconstrained for grand minima. The observational constraints on B-L type nonlinearity and stochasticity during grand minima are extremely limited, for the ARs are scarce. The generation of dipole moment for very weak cycles is lacking in the function we adopt, so a secondary peak for grand minima is missing in our probability density distribution, different from Usoskin et al. (2014). There are previous works suggesting that grand minima can be generated by stochasticity, for example, Choudhuri & Karak (2012); Olemskoy & Kitchatinov (2013); Karak & Miesch (2017). However, their analyses of the grand minima mainly focus on the total time of grand minima compared to all cycles, and do not cover whether or not the PDF of cycles is double-peaked as it is observed by Usoskin et al. (2014). From this perspective, the origin of grand minima is not clear at present. Better treatment of such weak cycles may produce better distribution containing more realistic grand minima in future work.

6. CONCLUSIONS

In this article, we produce an iterative map of solar cycle amplitude using the B-L type nonlinearity and stochasiticity based on observational properties of active regions. We use the iterative map to generate and analyze solar cycle amplitude series. We show that deterministic chaos is absent in our model regardless of model parameters, and stochasticity is always required to obtain solar cycle variability, which naturally limits the cycle prediction range. The distribution of synthetic cycles resembles the observed normal cycles, leaving the grand minima to be included in the model. The parameters of nonlinearity and stochasticity have profound influences on the distribution, and it can be inferred that the saturation of the B-L mechanism may have lower dipole moment saturating at higher cycle amplitude, as well as less stochasitcity compared to J20. Our result implies that with the amplitude of an ongoing cycle, the following cycle can be predicted but with uncertainty range, and that long-term prediction ahead of several cycles quickly loses its validity completely.

Generally, deterministic chaos cannot be present as long as, 1) the Ω-effect is mostly linear; 2) the Hale's polarity law is preserved; and 3) the generation of poloidal field follows a increase-then-saturate form. Furthermore, these requirements are not limited to Babcock-Leighton mechanism. Other type of quenched α-effects following these characteristics should also be devoid of chaos, and thus rely on stochasticity to generate varying cycle amplitudes. The reason is that if there is a fixed point at the saturation of the α-effects, the derivative of the recursion function always promotes its stability. In contrast, if the B-L mechanism or any form of α-effect actually decreases after reaching its peak with the increase of cycle amplitude as presented by Charbonneau et al. (2005), and the fixed points falls to the decreasing part, then chaos will be possible in the iteration map. This result can provide important guideline to future nonlinear solar dynamo model studies.

The authors acknowledge the utilization of the reconstructed sunspot number series by I. G. Usoskin, et al. (2014) (http://dx.doi.org/10.26093/cds/vizier.35629010), and the reconstructed sunspot number series by I. G. Usoskin, et al. (2021) (http://dx.doi.org/10.26093/cds/vizier.36490141). The International Sunspot Number version 2.0 is from the World Data Center SILSO, Royal Observatory of Belgium, Brussels, which is available at https://www.sidc.be/SILSO/datafiles. This research was supported by the National Natural Science Foundation of China through Grant Nos. 12425305, 12350004, 12173005, 12373111, & 12273061, the National Key R&D Program of China through Grant Nos. 2022YFF0503800, 2019YFA0405000, 2021YFA1600500, & 2022YFF0503000; the Strategic Priority Program of Chinese Academy of Sciences through Grant Nos. XDB41000000 & XDB0560000; and the Key Research Program of Frontier Sciences of CAS through Grant No. ZDBS-LY-SLH013. J.J. acknowledges the International Space Science Institute Team 474 for stimulating discussions.

REFERENCES

Balmaceda, L. A., Solanki, S. K., Krivova, N. A., & Foster, S. 2009, Journal of Geophysical Research (Space Physics), 114, A07104, doi: 10.1029/2009JA014299

Bhowmik, P., & Nandy, D. 2018, Nature Communications, 9, 5209, doi: 10.1038/s41467-018-07690-0

Biswas, A., Karak, B. B., & Cameron, R. 2022, PhRvL, 129, 241102, doi: 10.1103/PhysRevLett.129.241102

Cameron, R., & Schüssler, M. 2015, Science, 347, 1333, doi: 10.1126/science.1261470

Cameron, R. H., Jiang, J., & Schüssler, M. 2016, ApJL, 823, L22, doi: 10.3847/2041-8205/823/2/L22

Cameron, R. H., & Schüssler, M. 2016, A&A, 591, A46, doi: 10.1051/0004-6361/201527284

—. 2017, Astrophysical Journal, 843, 111, doi: 10.3847/1538-4357/aa767a

—. 2019, A&A, 625, A28, doi: 10.1051/0004-6361/201935290

Carbonell, M., Oliver, R., & Ballester, J. L. 1994, Astronomy and Astrophysics, 290, 983

Charbonneau, P. 2001, Solar Physics, 199, 385, doi: 10.1023/A:1010387509792

—. 2020, Living Reviews in Solar Physics, 17, 4, doi: 10.1007/s41116-020-00025-6

Charbonneau, P., & Dikpati, M. 2000, ApJ, 543, 1027, doi: 10.1086/317142

Charbonneau, P., St-Jean, C., & Zacharias, P. 2005, Astrophysical Journal, 619, 613, doi: 10.1086/426385

Choudhuri, A. R., Chatterjee, P., & Jiang, J. 2007, Physics Review Letters, 98, 131103, doi: 10.1103/PhysRevLett.98.131103

Choudhuri, A. R., & Karak, B. B. 2012, PhRvL, 109, 171103, doi: 10.1103/PhysRevLett.109.171103

Clette, F., Svalgaard, L., Vaquero, J. M., & Cliver, E. W. 2014, Space Science Reviews, 186, 35, doi: 10.1007/s11214-014-0074-2

Dasi-Espuig, M., Solanki, S. K., Krivova, N. A., Cameron, R., & Peñuela, T. 2010, Astronomy and Astrophysics, 518, A7, doi: 10.1051/0004-6361/201014301

Deng, L. H., Li, B., Xiang, Y. Y., & Dun, G. T. 2016, The Astronomical Journal, 151, 2, doi: 10.3847/0004-6256/151/1/2

Durney, B. R. 2000, Solar Physics, 196, 421, doi: 10.1023/A:1005285315323

Eddy, J. A. 1976, Science, 192, 1189, doi: 10.1126/science.192.4245.1189

Gleissberg, W. 1939, The Observatory, 62, 158

Gnevyshev, M. N., & Ohl, A. I. 1948, Astronomicheskii Zhurnal, 25, 18

Guo, W., Jiang, J., & Wang, J.-X. 2021, SoPh, 296, 136, doi: 10.1007/s11207-021-01878-2

Hanslmeier, A., & Brajša, R. 2010, Astronomy and Astrophysics, 509, A5, doi: 10.1051/0004-6361/200913095

Hathaway, D. H. 2015, Living Reviews in Solar Physics, 12, 4, doi: 10.1007/lrsp-2015-4

Hoyt, D. V., & Schatten, K. H. 1998, SoPh, 179, 189, doi: 10.1023/A:1005007527816

Jiang, J. 2020, Astrophysical Journal, 900, 19, doi: 10.3847/1538-4357/abaa4b

Jiang, J., Cameron, R. H., Schmitt, D., & Işık, E. 2013, A&A, 553, A128, doi: 10.1051/0004-6361/201321145

Jiang, J., Cameron, R. H., Schmitt, D., & Schüssler, M. 2011a, A&A, 528, A82, doi: 10.1051/0004-6361/201016167

—. 2011b, A&A, 528, A83, doi: 10.1051/0004-6361/201016168

Jiang, J., Cameron, R. H., & Schüssler, M. 2014a, Astrophysical Journal, 791, 5, doi: 10.1088/0004-637X/791/1/5

Jiang, J., & Cao, J. 2018, Journal of Atmospheric and Solar-Terrestrial Physics, 176, 34, doi: 10.1016/j.jastp.2017.06.019

Jiang, J., Chatterjee, P., & Choudhuri, A. R. 2007, Monthly Notices of the Royal Astronomical Society, 381, 1527, doi: 10.1111/j.1365-2966.2007.12267.x

Jiang, J., Hathaway, D. H., Cameron, R. H., et al. 2014b, SSRv, 186, 491, doi: 10.1007/s11214-014-0083-1

Jiang, J., Wang, J.-X., Jiao, Q.-R., & Cao, J.-B. 2018, Astrophysical Journal, 863, 159, doi: 10.3847/1538-4357/aad197

Jiao, Q., Jiang, J., & Wang, Z.-F. 2021, Astronomy and Astrophysics, 653, A27, doi: 10.1051/0004-6361/202141215

Karak, B. B. 2020, ApJL, 901, L35, doi: 10.3847/2041-8213/abb93f

—. 2023, Living Reviews in Solar Physics, 20, 3, doi: 10.1007/s41116-023-00037-y

Karak, B. B., & Miesch, M. 2017, ApJ, 847, 69, doi: 10.3847/1538-4357/aa8636

Kitchatinov, L. L., & Olemskoy, S. V. 2016, MNRAS, 459, 4353, doi: 10.1093/mnras/stw875

Knobloch, E., Tobias, S. M., & Weiss, N. O. 1998, MNRAS, 297, 1123, doi: 10.1046/j.1365-8711.1998.01572.x

Kumar, P., Karak, B. B., & Sreedevi, A. 2024, MNRAS, 530, 2895, doi: 10.1093/mnras/stae1052

Lean, J., Beer, J., & Bradley, R. 1995, Geophysical research letters, 22, 3195, doi: 10.1029/95GL03093

Li, K. J., Wang, J. X., Zhan, L. S., et al. 2003, Solar Physics, 215, 99, doi: 10.1023/A:1024814505979

Markwardt, C. B. 2009, in Astronomical Society of the Pacific Conference Series, Vol. 411, Astronomical Data Analysis Software and Systems XVIII, ed. D. A. Bohlender, D. Durand, & P. Dowler, 251, doi: 10.48550/arXiv.0902.2850

May, R. M. 1976, Nature, 261, 459, doi: 10.1038/261459a0

Mininni, P. D., Gómez, D. O., & Mindlin, G. B. 2000, Physical Review Letters, 85, 5476, doi: 10.1103/PhysRevLett.85.5476

Mundt, M. D., Maguire, W. Bruce, I., & Chase, R. R. P. 1991, Journal of Geophysical Research, 96, 1705, doi: 10.1029/90JA02150

Ohl, A. I., & Ohl, G. I. 1979, in NOAA Solar-Terrestrial Predictions Proceedings. Volume 2., ed. R. F. Donnelly, Vol. 2, 258–263

Olemskoy, S. V., & Kitchatinov, L. L. 2013, ApJ, 777, 71, doi: 10.1088/0004-637X/777/1/71

Parker, E. N. 1955, Astrophysical Journal, 122, 293, doi: 10.1086/146087

—. 1979, Cosmical magnetic fields. Their origin and their activity

Passos, D., Nandy, D., Hazra, S., & Lopes, I. 2014, A&A, 563, A18, doi: 10.1051/0004-6361/201322635

Petrovay, K. 2020, Living Reviews in Solar Physics, 17, 2, doi: 10.1007/s41116-020-0022-z

Petrovay, K., Nagy, M., & Yeates, A. R. 2020, Journal of Space Weather and Space Climate, 10, 50, doi: 10.1051/swsc/2020050

Price, C. P., Prichard, D., & Hogenson, E. A. 1992, Journal of Geophysical Research, 97, 19113, doi: 10.1029/92JA01459

Qin, L., Jiang, J., & Wang, R. 2024, ApJ, Under review

Rozelot, J. P. 1995, Astronomy and Astrophysics, 297, L45

Schatten, K. 2005, Geophysical Research Letters, 32, L21106, doi: 10.1029/2005GL024363

Schmalz, S., & Stix, M. 1991, Astronomy and Astrophysics, 245, 654

Solanki, S. K., Wenzler, T., & Schmitt, D. 2008, Astronomy and Astrophysics, 483, 623, doi: 10.1051/0004-6361:20054282

Steenbeck, M., Krause, F., & Rädler, K. H. 1966, Zeitschrift Naturforschung Teil A, 21, 369, doi: 10.1515/zna-1966-0401

Svalgaard, L., Cliver, E. W., & Kamide, Y. 2005, Geophysical Research Letters, 32, L01104, doi: 10.1029/2004GL021664

Talafha, M., Nagy, M., Lemerle, A., & Petrovay, K. 2022, Astronomy and Astrophysics, 660, A92, doi: 10.1051/0004-6361/202142572

Tobias, S. M., Weiss, N. O., & Kirk, V. 1995, MNRAS, 273, 1150, doi: 10.1093/mnras/273.4.1150

Usoskin, I. G., Solanki, S. K., Krivova, N. A., et al. 2021, Astronomy and Astrophysics, 649, A141, doi: 10.1051/0004-6361/202140711

Usoskin, I. G., Hulot, G., Gallet, Y., et al. 2014, Astronomy and Astrophysics, 562, L10, doi: 10.1051/0004-6361/201423391

Wang, Y. M., & Sheeley, N. R., J. 1991, Astrophysical Journal, 375, 761, doi: 10.1086/170240

Wang, Z.-F., Jiang, J., & Wang, J.-X. 2021, A&A, 650, A87, doi: 10.1051/0004-6361/202140407

Weber, M. A., Fan, Y., & Miesch, M. S. 2013, SoPh, 287, 239, doi: 10.1007/s11207-012-0093-7

Wilmot-Smith, A. L., Martens, P. C. H., Nandy, D., Priest, E. R., & Tobias, S. M. 2005, MNRAS, 363, 1167, doi: 10.1111/j.1365-2966.2005.09514.x

Yeates, A. R., Bertello, L., Pevtsov, A. A., & Pevtsov, A. A. 2024, arXiv e-prints, arXiv:2412.02312, doi: 10.48550/arXiv.2412.02312

Yeates, A. R., Cheung, M. C. M., Jiang, J., Petrovay, K., & Wang, Y.-M. 2023, SSRv, 219, 31, doi: 10.1007/s11214-023-00978-8

Yoshimura, H. 1978a, Astrophysical Journal, 220, 692, doi: 10.1086/155953

—. 1978b, Astrophysical Journal, 221, 1088, doi: 10.1086/156112